Proceedings World Geothermal Congress 2023
Beijing, China, April 17 – 21, 2023

CO_2-Brine-Rock Interactions under Long-term High Pressure High Temperature Reactor Treatment of Kızıldere Geothermal Reservoir Rocks

Agrawal H.[1], Lathouri M.[1], Cao W.[1], Korre A.[1], Durucan S.[1], Parlaktuna M.[2], Sinayuc C.[2], Wolf K-H.[3]

[1]Department of Earth Science and Engineering, Royal School of Mines, Imperial College London, London, SW7 2AZ, UK

[2]Department of Petroleum and Natural Gas Engineering, Middle East Technical University, Ankara, Turkey

[3]Department of Applied Geophysics and Petrophysics, Delft University of Technology, Zuid-Holland, The Netherlands

h.agrawal17@imperial.ac.uk / hagrawal6@gmail.com

Keywords: Geothermal systems, High-pressure high-temperature, Reservoir properties, CO_2-brine-rock interactions, Carbon capture, utilisation and storage (CCUS).

ABSTRACT

The geothermal energy sector is on a rise in several countries as geothermal reservoirs provide a source of renewable energy, as well as the means to permanently lock CO_2 into the reservoir rocks for thousands of years. Geological storage of CO_2 in geothermal reservoirs should be investigated for the success of the long-term implementation of the coupled geothermal-CO_2 injection technology. The complex CO_2-brine-rock interactions, which can affect the geochemical, geomechanical and geophysical properties of reservoir rocks, have implications on the CO_2 storage potential of the reservoir and affect the efficiency of the long-term carbon storage. A new long-term high-pressure high-temperature laboratory reactor experiment has been designed and implemented, and results have been analysed to characterise the changes in structural, hydrogeological and geomechanical properties of the reservoir rocks and the geochemistry of the reactor fluids when in contact with CO_2. The geochemical reactions occurring within the Kızıldere geothermal reservoir have been modelled using PHREEQC, the results from preliminary analysis match well with the field conditions and those reported by previous researchers.

1. INTRODUCTION

Geothermal energy offers a cheap, clean and sustainable source of renewable energy that can be utilised for a variety of domestic and industrial applications (ESMAP, 2016). Geothermal wells situated in carbonate reservoirs (like those in Turkey) contain a significant amount of non-condensable gases including carbon dioxide (CO_2) (Satman et al., 2020) and smaller amounts of ammonia (NH_3), nitrogen (N_2), methane (CH_4), hydrogen sulphide (H_2S) and hydrogen (H) in the produced steam. A high geothermal fluid-flow rate is required in power plants leading to venting a large volume of CO_2 to the atmosphere (Holm et al., 2012). Layman (2017) reports that a 50 MWe geothermal project in Turkey can emit up to 1,200 tonnes of CO_2 per day in the atmosphere. The produced fluid (depleted in CO_2) is reinjected into the geothermal reservoir gradually diluting the CO_2 content, this in turn affects the field productivity due to decreased wellhead flowing pressure and temperature (Satman et al., 2020).

Reinjection of supercritical CO_2 back into the geothermal fields has been proposed by several researchers (Pruess, 2006; Wallace et al., 2009; Salimi and Wolf, 2012; Aksoy et al., 2015; Haizlip et al., 2016; Sun et al., 2016; Peter et al., 2022; Wang et al., 2022) to enhance geothermal production and address the current climate-change challenge through CO_2 utilisation and storage. The injected CO_2 reacts with the formation brine resulting in a low pH environment (Wang et al., 2022). CO_2-brine-rock interactions affect the geochemical, geomechanical and geophysical properties of carbonate rocks through the dissolution of calcite, as reported by several researchers (Sun et al., 2016; Pimienta et al., 2017; Valle et al., 2020; Peter et al., 2022). Most researchers used reactor treatment in which the core samples were exposed to simulated *in situ* pressure-temperature conditions to represent the natural geothermal field conditions. Most of these studies were conducted in the temperature range of 10-70 °C and pressure range of 3-150 MPa owing to experimental limitations and for a short-term, ranging from a few days to weeks (Sun et al., 2016; Pimienta et al., 2017; Jahanbakhsh et al., 2018; Jahanbakhsh et al., 2021; Peter et al., 2022). A detailed review of reactor treatment experiments conducted around the world was presented by Sun et al. (2016).

As CO_2 resides in the geothermal reservoir for thousands of years, long-term CO_2-brine-rock interaction is expected. This may lead to dynamic changes in pressure and temperature, affect CO_2 solubility and result in different phases of CO_2 (including free and mobile CO_2) (Sun et al., 2016; Satman et al., 2020; Peter et al., 2022). Long-term analysis of CO_2-brine-rock interactions on the geochemical, geomechanical and geophysical properties of rocks, as well as its implications on the CO_2 storage capacity of the reservoir and efficiency of the storage process, is necessary for the success of the long-term application of the coupled geothermal-CO_2 injection technology. To obtain an improved understanding of supercritical CO_2-brine-rock interactions and their impacts on reservoir rocks, CO_2-brine-rock interaction experiments were conducted by maintaining high-temperature and high-pressure for a prolonged 16 months period on reservoir rock samples sourced from the Kızıldere geothermal field.

The Kızıldere geothermal field located in the East of Büyük Menderes graben in Western Anatolia was discovered in 1968 as the first site with a potential for geothermal energy in Turkey (Akin et al., 2003; Garg et al., 2015). It has two main reservoirs, the first made up of limestones of the Sazak formation, and the second within marble-gneisses-quartzite-schist intercalations of the Igdecik and Paleozoic formations (Şimşek et al., 2005; Haklıdır et al., 2011; Satman et al., 2020), which carry a significant amount of dissolved CO_2 (over 3% by weight depending on the depth). The reservoir properties may vary depending on the mineral composition, microstructure, fractures induced during the geological history of the rock, temperature, pressure, water chemistry, CO_2 phase, etc. (Peter et al., 2022). The geothermal fluid present in the Kızıldere geothermal reservoir was mostly saturated with CO_2 in its natural

state. The geochemical composition of the fluid previously analysed (Haklıdır et al., 2015) was considered to prepare the synthetic brine used in the experiments. The temperature and pressure conditions were maintained close to that at the bottom hole of the geothermal wells to replicate the geothermal reservoir conditions.

2. METHODOLOGY

As reported by previous researchers, CO_2-brine-rock interactions can cause geochemical, geomechanical and geophysical changes in the rock samples. For instance, Hao et al. (2013) found that CO_2 saturated brine can create wormholes inside the rock samples due to the dissolution of minerals in an acidic solution. Tan et al. (2022) observed an increase in pore size due to the dissolution of calcite minerals and subsequent precipitation of carbonates decreasing the pore size. They also observed acid etching on the rock surface (surface corrosion) due to CO_2-brine-rock interactions. Peter et al. (2022) reported a change in the elemental composition of the rock sample due to reactivity with CO_2-brine, and the presence of brine often accelerates such changes. This can be evaluated by different laboratory testing methods to understand the change in micro-fabric, morphology and elemental composition of minerals present in the rock and the change in geomechanical and geophysical properties of rock due to the long-term CO_2-brine-rock interactions.

During the first stage of the laboratory experiments, large number of marble core samples representative of the deep reservoir in Kızıldere were characterised for their baseline reservoir properties and exposed to high pressure high temperature brine solution charged with CO_2 at subsurface reservoir conditions. At the time of preparing this paper, one reactor cell (housing 3 marble samples) was opened to analyse the effects of exposure to reservoir brine and CO_2 on the cores and the brine geochemistry. The remaining twelve marble cores housed in four reactor cells are being exposed to CO_2 depleted brine at high pressure and temperature, representing re-injection of the spent reservoir fluid as implemented in the field. The last stage of the reactor experiments will aim at simulating CO_2 re-injection in the reservoir. This paper reports on the results obtained from the first stage experiments described in detail. The complete analysis of the experimental data on 15 marble samples and the changes observed on marble properties and brine geochemistry will be published in due course, after the completion of the third stage experiments.

3. BASELINE CHARACTERISATION OF THE RESERVOIR ROCKS

3.1. Sample preparation

Large marble blocks sourced from fresh outcrops around the Kızıldere geothermal field, representing the deep reservoir in Kızıldere were cored, cut, and polished as twenty-four 38 mm core samples for laboratory experiments (Figure 1a). After CT-scanning, these cores were tested to characterise baseline reservoir properties such as porosity and permeability. Five of these cores were taken through multistage triaxial testing to determine representative mechanical and elastic properties of the marble reservoir rock. Fifteen of these cores were placed in five reactor cells (each with 3 marble cores) and exposed to high pressure high temperature brine solution charged with CO_2 at subsurface reservoir conditions for a period of 16 months. Four core samples were reserved for confirmatory analysis if required.

(a) (b)

Figure 1: (a) Large marble block representative of the deep reservoir in Kızıldere, and (b) Cored and polished marble samples for laboratory experiments.

3.2. X-ray diffraction (XRD) analysis

In X-ray diffraction analysis, a small amount of powdered rock sample is used. The sample is placed under a beam of X-rays that hit the sample at a slowly increasing angle (Setiawan et al., 2018). The diffracting X-ray beam is detected using an electronic detector that keeps rotating around the sample. An X-ray diffraction pattern is recorded for each sample with a series of peaks occurring at different heights. These peaks correlate with the atomic spacing in mineral crystals and are compared with an extensive database of minerals to determine the presence of different minerals in the rock sample. An XRD analysis was conducted to identify the mineral composition of Kızıldere marble samples (Table 1). The analysis showed that the bulk composition was a mixture of calcite and dolomite.

3.3. Micro-computed tomography (μ-CT)

μ-CT scanning is a non-destructive technique in which X-ray scanners are used to scan rock samples and generate a large number of cross-sectional 2D images (Nehler et al., 2015; Sun et al., 2016; Jahanbakhsh et al., 2021). Reconstruction algorithms are used to combine these 2D images to generate a 3D image (at >100 μm scale) to analyse the interior of the rock. Commercial software can be used on these 3D images to determine the change in geochemical (Jahanbakhsh et al., 2021) and geophysical (Nehler et al., 2015) properties of rock in repeat scans. All twenty-four intact marble core samples were scanned using a Phoenix Nanotom™ Micro-CT

scanner with a ca. 50 - 25 micron scale resolution. A marble core sample with a visible iron stained filling is shown in Figure 2a, and the corresponding μ-CT scans illustrating the orientation and extent of the fracture are presented in Figure 2b.

Table 1: Chemical composition of Kizildere marble samples.

	(%wt)
Aluminium oxide (Al_2O_3)	0.180
Calcium oxide (CaO)	97.200
Cupric oxide (CuO)	0.041
Ferric oxide (Fe_2O_3)	0.330
Lead oxide (PbO)	--
Magnesium oxide (MgO)	1.220
Nickel oxide (NiO)	0.036
Phosphorous pentoxide (P_2O_5)	0.030
Potassium oxide (K_2O)	0.021
Silicon dioxide (SiO_2)	0.800
Sodium oxide (Na_2O)	0.025
Strontium oxide (SrO)	0.018
Titanium dioxide (TiO_2)	--
Zinc oxide (ZnO)	0.025
Sulphite ion (SO_3^{2-})	0.041
Chloride ion (Cl^-)	0.039

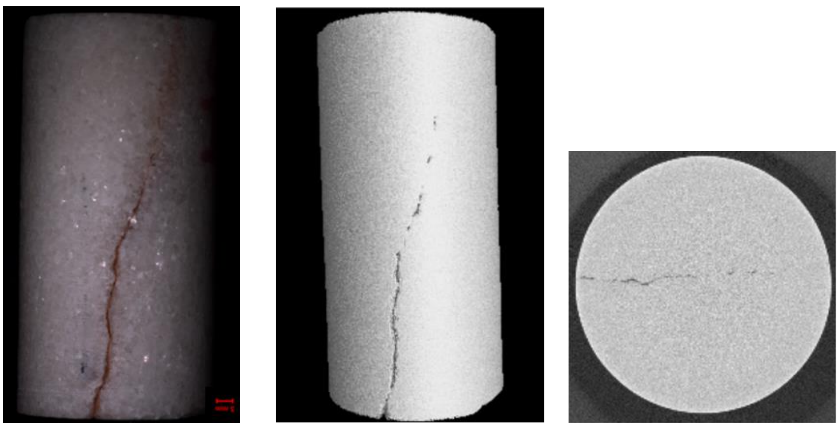

(a) (b)

Figure 2: (a) Fractured marble – core sample C-I and (b) μ-CT image of the same sample before the long-term HPHT reactor treatment experiments.

3.4. Porosity measurements

Porosity, a measure of the space available in the rock sample for fluid storage, was determined using a Helium Pycnometer (Figure 3a). A series of helium expansion calculations were performed to calculate the volume of gas occupied in the pores of the rock sample against the dead volume of the system using Boyle's law,

$$P_i V_i = P_f V_f \tag{4}$$

where P_i is the initial pressure (Pa), P_f is the final pressure (Pa), V_i is the initial volume (cm^3), and V_f is the final volume (cm^3).

3.5. Permeability measurements

Permeability, the ability of a rock to transmit fluid under pressure differential, is measured using a modified high-pressure Hassler cell (Figure 3b) (Hassler, 1944). Darcy's equation for compressed gases is used to calculate the permeability coefficient of the samples assuming that the gas flow through the rock is under isothermal conditions. The axial permeability can be calculated as (Koederitz et al., 1989; Zhang et al., 2021; Zhang et al., 2015),

$$k = 2\xi Q P_2 l_s / A(P_1^2 - P_2^2) \tag{5}$$

where k is the permeability coefficient (m^2), Q is the volumetric flow rate (m^3/s), ξ is the dynamic viscosity (Pa-s), l_s is the length of the cylindrical core (m), A is the cross-sectional area of the cylindrical core (m^2), P_1 is the upstream pressure (MPa), and P_2 is the downstream pressure (MPa).

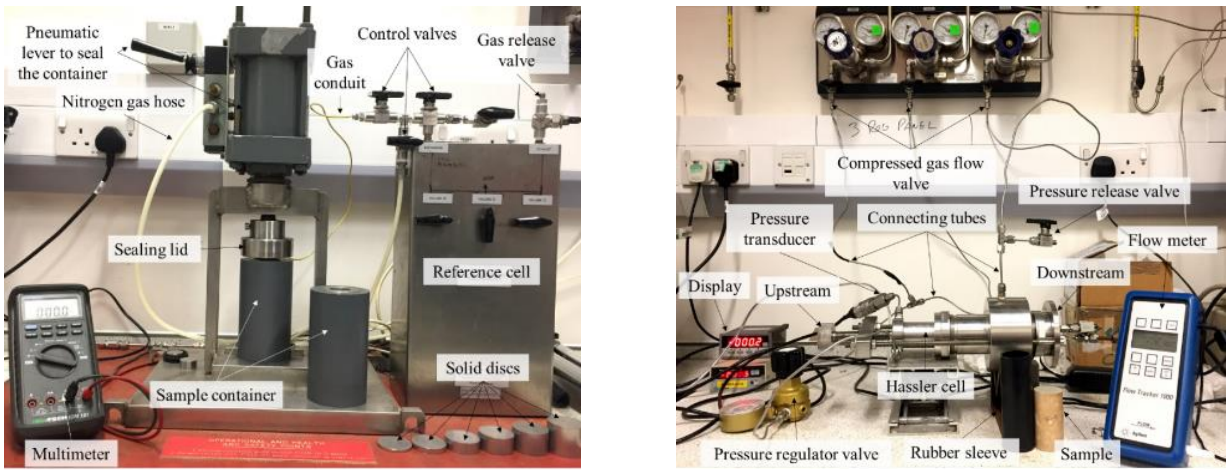

(a) (b)

Figure 3: Experimental set-up of (a) Helium Pycnometer used for porosity of the core samples and (b) Hassler cell used to measure the permeability of the core samples.

3.6. Multi-stage triaxial testing

Multistage triaxial testing of the solid core samples was performed in a four-column 2,000 kN capacity, servo-controlled, stiff rock testing system by ESH Testing Limited, Brierley, UK (Figure 4a), to determine the stress-strain response of the rock to axial load, and to characterise geomechanical properties (Kovari and Tisa, 1975). The axial displacement of the loading platen is monitored by two LVDT (linear variable differential transformers) connected externally. The strain gauge readouts and the LVDTs are connected to the servo-controlled system. The hydrostatic and deviatoric stresses are controlled independently using the servo-controlled system. The confining pressure is manually controlled using a pressure regulator fitted to the hydraulic pump and is monitored using an electronic pressure transducer with a display. The multistage triaxial testing is performed by increasing the confining pressure in stages (at 1.5, 5.0, 8.0, and 14.0 MPa, before finally being brought to failure at 18.0 MPa confinement). At each stage, the confining pressure is kept constant, and the axial load is increased at a constant strain rate of 1.5 mm/hr until the sample starts to yield, at which point the axial load is stopped and the confining pressure is increased to the next stage using the hydraulic pump. This process is repeated, and the sample is subsequently brought to failure at the final confining stage to measure the ultimate compressive strength of the sample. The axial stress, axial strain, and lateral strain are continuously recorded during the experiment.

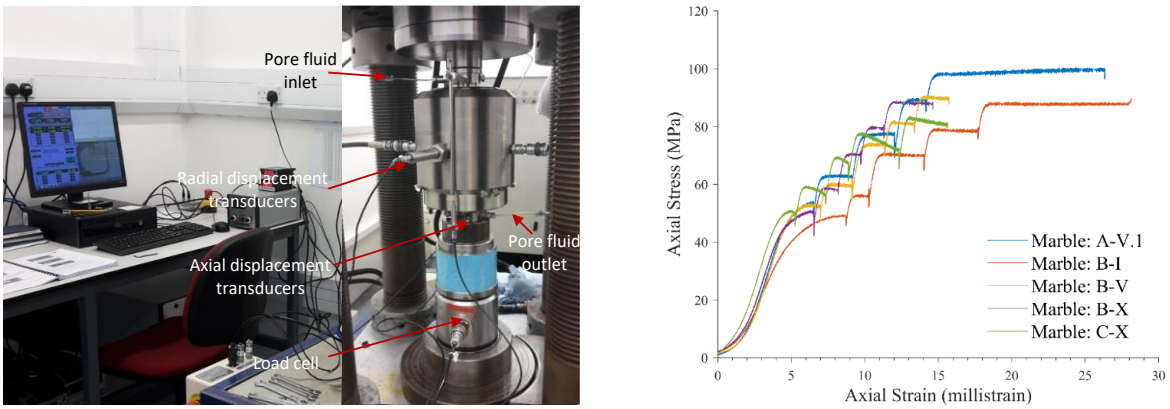

(a) (b)

(c)

Figure 4: (a) Experimental set-up for multistage triaxial testing (b) the stress-strain plots for the five marble samples under multistage triaxial testing, and (c) failed marble samples in multi-stage triaxial testing.

Table 2: Laboratory determined geomechanical and reservoir properties of reservoir marbles tested.

Sample	l_s	D	w_s	*V*	GD	φ	k	E	υ	c	ϕ	σ_c	σ_{max}
Marble A-VI	74.86	36.83	215.00	79.80	2.55	5.7	5×10^{-18}	15.40	0.29	13.2	31.0	46.66	101.46
Marble B-I	75.16	36.63	214.65	79.23	2.56	5.8	2×10^{-18}	10.83	0.18	13.0	27.5	42.84	89.78
Marble B-V	75.17	36.60	214.56	79.12	2.41	12.6	2×10^{-18}	14.79	0.27	13.5	28.5	45.38	90.82
Marble B-X	75.09	36.56	213.83	78.85	2.49	8.6	3×10^{-18}	15.20	0.31	13.2	28.0	43.93	88.94
Marble C-X	73.37	36.62	208.75	77.30	2.53	6.9	2×10^{-18}	15.64	0.24	13.5	27.5	44.49	83.66

l_s is the length (mm), D is the diameter (mm), w_s is the weight (g), *V* is the volume (mm^3), GD is the grain density (g/cc), φ is the porosity (%), k is the permeability (m^2), E is Young's modulus (GPa), υ is the Poisson's ratio, c is the cohesion (MPa), ϕ is the angle of internal friction (°), σ_c is the unconfined compressive strength (MPa) and σ_{max} is the peak strength of the sample at 18.0 MPa confinement (MPa).

Table 2 presents the geomechanical and gas flow properties of the five Kızıldere marbles tested. The permeability of all marble samples was in the nano-Darcy range confirming that flow in the reservoir is mainly through fractures and faults. The stress-strain plot for the marble samples follow a similar trend during the experiment (Figure 4b). The samples exhibit ductile behaviour and show a clear plateau at each confinement level. The stress acting on each marble sample is comparable with slight variations observed. Marble A-VI experienced plastic failure (at maximum peak strength) while other samples failed in shear upon multistage triaxial testing (Figure 4c).

3.7. High-pressure high-temperature reactor set-up

The laboratory set up constructed for the long-term high pressure high temperature experiments is shown in Figure 5. Hastelloy vessels of 40 mm diameter and 270 mm length, referred to as the HPHT reactors, were used for the reactor treatment experiments. Each reactor was designed to house 3 samples along their length and provide an annular space to accommodate synthetic brine representing the Kızıldere reservoir brine. The reactors were constructed with an inlet to inject synthetic brine and CO_2 and an outlet to bleed air, monitor and release excess pressure from the vessel. The reactor inlet was connected to an isolation manifold to isolate each reactor from the system as and when needed. The synthetic brine was stirred continuously on a magnetic stirrer at 20 °C overnight to ensure a uniform brine concentration before injection into the reactor. The brine and gas pressure regulator was connected to an ISCO syringe pump through a T-connection and an isolation valve to pump brine and CO_2 gas at required pressure into each reactor by operating the isolation valves. The HPHT reactors were placed inside a temperature-controlled oven to maintain a constant temperature throughout the experiment.

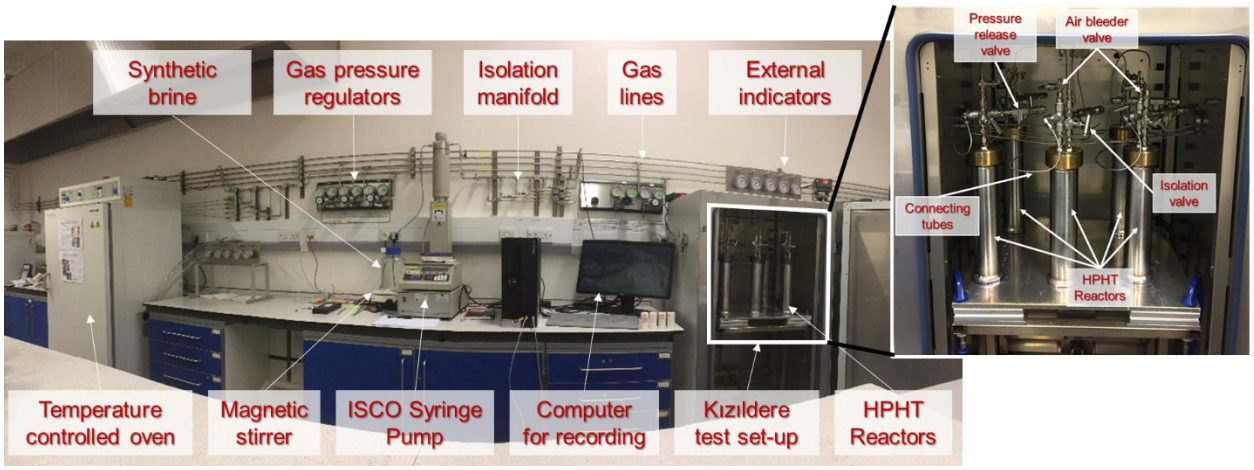

Figure 5: Laboratory set up for the long-term high pressure high temperature experiments.

Three marble cores were placed in each reactor with the inlet and outlet of the reactors connected as designed. The experimental set-up was pressure tested at 2,500 psi for several days to ensure that there is no leakage, and that the reactor is holding the pressure. Synthetic brine was introduced into the annular space of the reactor keeping the air bleeder valve open to bleed air present in the reactor. Once the reactor was completely filled with brine, the air bleeder valve was closed. The feedline was cleared of brine by purging nitrogen through it, before pushing CO_2 into the reactor. CO_2 (equivalent to 4 % by weight) was introduced into the reactor and the reactors were isolated for 24 hours to saturate the brine. The volume of synthetic brine and CO_2 present in each reactor is listed in Table 3. The temperature of the oven was increased in steps of 25 °C and equilibrated overnight before increasing the temperature. The final temperature and pressure of the oven was maintained at 200 °C and 2,000 psi, respectively. The pressure gauge connected to the outlet along with the pressure transducer with display was remotely monitored daily using the computer assembly to record the temperature and pressure inside the HPHT reactor (Figure 5). Five such HPHT reactors were connected through the isolation manifold to the system to accommodate 15 marble samples for the long-term experiments.

Table 3: The volume of brine and carbon dioxide injected into each reactor to maintain a 4 %wt saturation.

Vessel no.	V_{brine}	V_{CO2}
Vessel 1	308.20	6235.63
Vessel 2	307.75	6226.66
Vessel 3	308.22	6236.06
Vessel 4	308.32	6238.23
Vessel 5	310.73	6286.98

V_{brine} is the volume of brine in reactor (ml), and V_{CO2} is the volume of CO_2 injected in each reactor (ml).

The Kızıldere geothermal field consists of convecting fluid mixture that flows in its natural state, the scale of such convection is in the order of 10^4 years. Thus, natural state during which geothermal energy exploitation is planned (10-50 years) can be considered stationary (Garg et al., 2015). During exploration and early stages of development, natural production fluid flow will be dominant. Thus, static experiments were performed in the reactor treatment experiments to bring the samples to the initial reservoir conditions which existed before geothermal fluid production first started in the field. As solubility of CO_2 is highly sensitive to pressure and temperature changes, a constant pressure and temperature condition was maintained in the reactors during the experiments.

4. GEOCHEMICAL CHARACTERISATION OF RESERVOIR FLUIDS

4.1. Hydrochemical characterisation

Graphical representation of major dissolved constituents in groundwater helps in understanding their hydrochemical evolution, grouping and areal distribution. The Piper diagram is a useful graphical tool to represent and classify surface and groundwater based on their geochemical characteristics, and the presence of major cations and anions (Piper, 1944). The diagram consists of two base triangles, with major cations (Ca^{2+}, Mg^{2+}, Na^{+}, K^{+}) plotted on the left triangle and major anions (Cl^{-}, SO_4^{2-}, CO_3^{2-}, HCO_3^{-}) plotted on the right triangle, illustrating different water types. The overall information from the two triangles is combined in a central diamond-shaped field, representing a projection of the two triangles by one single point. This single point depends on the concentration of different cations and anions relative to each other and is thus uniquely related to the total ionic relationship. The illustration provides insights into the chemical and physical processes that control water chemistry. Based on these diagrams, and their evolution, any changes in the hydrochemical processes through space and time can be identified. The geochemical characteristics of the fluid present in the Kızıldere geothermal field were evaluated on Piper diagrams.

Table 4: Initial chemical composition of the geothermal fluid in the production and reinjection wells (after Haklıdır et al., 2015) and estimated partial pressure of carbon dioxide assuming carbonate equilibria at temperature (this study).

Well ID	T	P	pH	K^+	Na^+	Ca^{2+}	Mg^{2+}	Fe	SiO_2	CO_3^{2-}	HCO_3^-	SO_4^{2-}	Cl^-	pCO_2
KD-23B	245	230/285	6.9	228	1304	1.33	<1	0.08	697	<10	2515	653	110	4.61
KD-23D	238	215/178	6.7	209	1295	1.08	<1	0.05	503	<10	2487	591	104	4.77
KD-18A	215	195	7	220	1165	1.45	<1	<0.05	552	<10	2577	638	115	3.57
KD-2A	230	168/160	7.6	204	1305	1.96	<1	0.05	682	<10	2624	588	115	2.16
KD-9A	205	210	6.7	184	1158	1.36	<1	<0.05	520	<10	2379	524	92.9	3.84
R-1A	230	165	6.7	183	1135	1.3	<1	0.05	601	<10	2420	620	107	4.49
R-3A	240	185	7.2	347	1278	4.41	<1	<0.05	732	<10	2990	623	122	4.39
R-5A	220	215/190	6.8	165	1147	1.19	<1	<0.05	469	<10	2338	572	101	3.91
KD-38A	175/149	225/166	8.2	107	1001	1	1.23	0.07	402	138	1729	577	92.9	0.09
KD-38C	142	92	6.3	111	800	24.7	4.91	0.3	364	<10	1573	497	90	2.05
KD-28A	145	210	6.8	140	977	46.1	9.12	0.5	229	<10	2049	574	94.4	1.57
KD-27A	185	215	7.3	175	1086	1.37	1.39	<0.05	315	<10	2204	472	77.1	1.43
KD-25A	223	222	6.75	142	1100	3.66	1.06	<0.05	578	<10	2267	597	95.7	3.98
Kar	-	-	7.5	130	859	4.37	9.23	0.09	115	<10	1903	458	85.8	0.05
KD-35	-	-	6.6	96.8	836	39.1	9.29	0.2	115	<10	1637	559	118	0.25
KD-33	138	130	7	104	555	131	15.4	0.2	302	<10	1432	515	65.6	0.73
KD-32A	138	130	7.2	70.5	466	226	35	0.3	250	<10	1362	629	60.9	0.47

T is the bottom-hole temperature (˚C), P is the bottom-hole pressure (barg), with the two numbers indicating static/dynamic temperature and/or pressure respectively. pH is the potential of Hydrogen measured at 20-22 ˚C, K^+ is the Potassium ion concentration (mg l^{-1}), Na^+ is the Sodium ion concentration (mg l^{-1}), Ca^{2+} is the Calcium ion concentration (mg l^{-1}), Mg^{2+} is the Magnesium ion concentration (mg l^{-1}), Fe is the Iron concentration (mg l^{-1}), SiO_2 is the Silicon dioxide concentration (mg l^{-1}), CO_3^{2-} is the Carbonate ion concentration (mg l^{-1}), HCO_3^- is the Bicarbonate ion concentration, SO_4^{2-} is the Sulphate ion concentration (mg l^{-1}), Cl^- is the Chloride ion concentration (mg l^{-1}). pCO_2 is the partial pressure of carbon dioxide in the well (barg) estimated in this study.

The geochemical composition of the fluid present in the Kızıldere geothermal field is listed in Table 4 after Haklıdır et al. (2015). Ionic concentrations for Mg^{2+} and CO_3^{2-} were found to be below the limit of detection (LOD), hence, these values were substituted with a constant value, such as one-half the limit of detection ($1/2$ LOD). This is the simplest and most commonly used method for handling below detection limit values. Major ion concentrations present in the fluid were plotted on Piper diagrams and used to classify the reservoir fluids previously analysed from seventeen Kızıldere wells (Figure 6). The chemistry of geothermal fluids falls

into two different hydrochemical types, $Na - HCO_3$ and $Na - Cl - SO_4$. The change in ionic composition of fluids might be due to two different groundwater sources, temperature-dependent dissolution/ precipitation of ions in their flow path, mixing of surface water with underground aquifer or contamination by saline water. It is evident that the bicarbonate-rich water types originate possibly from the inflow of magmatic gases in the geothermal reservoir and incomplete neutralisation of such fluids through either dissolution of CO_2-bearing gases or condensation of geothermal steam in relatively deep, oxygen-free ground waters, as the absence of oxygen prevents oxidation of H_2S. The acidity of these aqueous solutions is due to the dissociation of carbonic acid (H_2CO_3). Carbonate (CO_3^{2-}) and bicarbonate (HCO_3^-) buffered solutions are the most common examples of the aqueous reactions that could affect the geochemistry of the system.

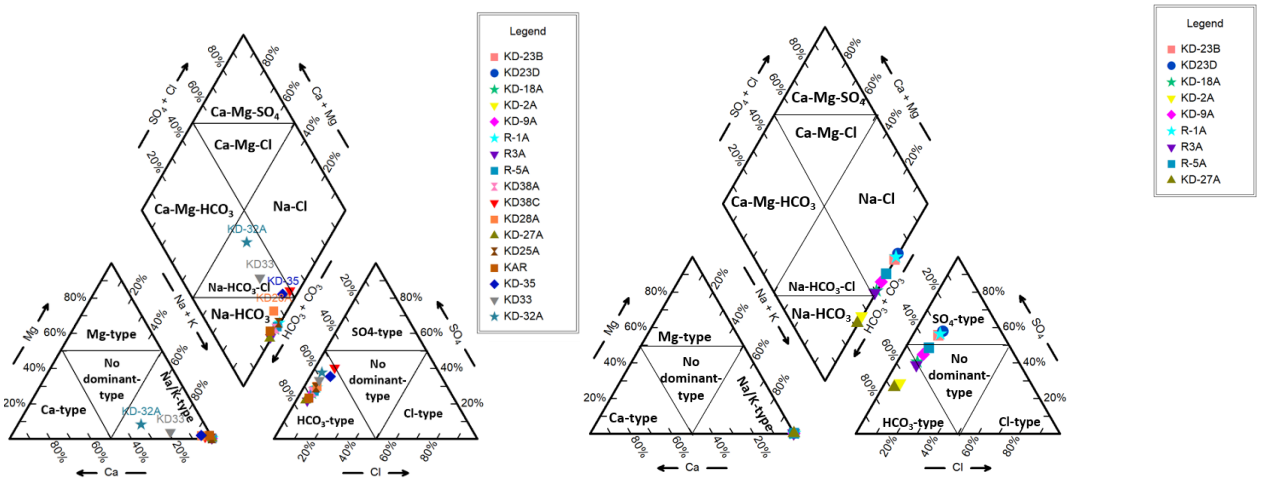

Figure 6: Hydro-geochemical characteristics of thermal water determined using the Piper diagram for, (a) all production and reinjection wells and (b) all observation and reinjection wells.

Sodium chloride (NaCl) is the predominant salt component present in dissolved form adding salinity to geothermal fluids. It is indicative that higher Na^+ and Cl^- ion concentrations correspond to a higher temperature. Especially the presence of Cl^- ion concentration determines the dilutions or contribution/ outflow of deep thermal fluids (Shah et al., 2018). The $Na - Cl - SO_4$ fluid type may be explained by the mixing of acidic (SO_4^{2-}) fluids with neutral NaCl (saline brines) aquifers, as geothermal fluids usually contain high dissolved salts and ion concentrations. The dominance of SO_4^{2-} over HCO_3^- suggests that the thermal fluids might have been mixed with marginal steam heated fluid or during the fluid-rock interaction, interacting with the sulfur-bearing environment.

4.2. Geochemical equilibrium modelling

For the geochemical modelling, PHREEQC, a well-known geochemical software that can model complicated reactions occurring in fluid-rock interaction systems by considering the equilibrium between gaseous, aqueous, and solid phases was used (Pham et al., 2011; Parkhurst and Appelo, 2013; Zhu et al., 2013; Shabani et al., 2019; Zou et al., 2021; Wang et al., 2022). PHREEQC is based on the ion association model and uses the Peng-Robinson equation of state to model non-ideal gas behaviour to estimate the solubility of gases at high pressure (Parkhurst and Appelo, 2013; Tale et al., 2020). The latest version of PHREEQC (version 3) has many beneficial features to model the geochemical reaction kinetics at a different temperature, pressure and composition of fluids and the dissolution of minerals occurring in CO_2-brine-rock systems (Appelo and Postma, 2005; Pham et al., 2011; Nehler et al., 2015; Shah et al., 2018; Zhang et al., 2020; Wang et al., 2022).

The critical pressure and temperature were defined for a gas component and the Peng-Robinson equation of state was used to calculate the relation between pressure and molar volume and the fugacity coefficient for CO_2 gas. For dissolved ideal gases in equilibrium with the solution, the saturation index (SI) is defined as $SI = \log(\text{fugacity})$, where fugacity equals partial pressure (pCO_2) of the gas. Initial partial pressure, along with volume and temperature was used to calculate the initial moles of CO_2 gas component in the fixed-pressure gas phase, in equilibrium with an aqueous solution. The program then uses the CO_2 gas phase in contact with the fluid and distributes the gas components between the aqueous and the gaseous phase. CO_2 was therefore modelled, setting the initial gas component partial pressure of 3 atm, under fixed-pressure and fixed-volume conditions. This estimated a CO_2 concentration of 0.1 mol l^{-1} or 4.4 g l^{-1}, which is consistent with literature values (Addassi et al., 2021; Satman, 2020; Satman et al., 2017).

The thermodynamic database (pitzer.dat), available with the PHREEQC model release, was utilised to model the geothermal fluids speciation because of their high ionic strength (Appelo et al., 2014). The sum of all CO_2, $HCO_3^-$and CO_3^{2-} species was considered as total CO_2 (total dissolved inorganic carbon) to start the calculations. PHREEQC was then set up to adjust CO_2 to be in equilibrium with the solution, until it reaches a saturation index of 0.50, equal to 3 atm, since $\log_{10}(pCO_2) = SI_{CO_2}(g)$. An initial CO_2 concentration of 0.029 mol l^{-1} (i.e., 1.28 g l^{-1}) was fed into PHREEQC to calculate the distribution of ions. PHREEQC was also used to determine the mineral saturation indices (SI). These specify the reaction of each phase, representing dissolution, precipitation or equilibrium condition when brought into contact with an aqueous solution (Zhu and Anderson, 2002):

- $SI = 0$, the mineral is in equilibrium with the solution,
- $SI > 0$, the mineral is supersaturated, the capacity of the considered mineral to precipitate,
- $SI < 0$, the mineral is undersaturated, the capacity of the water to dissolve the considered mineral, when in contact with water.

PHREEQC (version 3) was used to simulate the geochemical reactions taking place, using the Pitzer model for the high salinity brines, and determine the pressure dependence equilibrium constant for aqueous ions (Rose et al., 2007; Parkhurst and Appelo, 2013). The Debye-Hückel equation or the Davies equation (Appelo and Postma, 2005) can be applied for ionic strength corrections on selected thermodynamic databases. The equilibrium condition is estimated when the mass action equations lead to the minimum Gibbs free energy (Parkhurst and Appelo, 2013; Zou et al., 2021). The equilibrium constant (log K) can be calculated as a function of temperature (T) as,

$$log\, K = -1.134 - 1.363 \times 10^{-2}T + 6.614 \times 10^{-5}T^2 - 1.286 \times 10^{-7}T^3 + 7.348 \times 10^{-11}T^4 \quad (1)$$

As a first step, the PHREEQC (version 3) geochemical equilibrium model was used to calculate the salt concentration that ought to be dissolved in the synthetic brine for use in long-term high pressure high temperature laboratory experiments. In addition to ion exchange and precipitation dissolution mechanisms, the reaction between gaseous and aqueous phases was also incorporated into the modelling. When modelling static CO_2-brine-rock interactions, constant volume and temperature, no mechanical trapping of gases and no leakage in the system were assumed. As brine is saturated with CO_2 and the rock is immersed in brine, dissolved CO_2 reacts with the rock. Gas solubility in brine is the main concern in modelling a brine-gas interaction system (Wang et al., 2022). In PHREEQC, the solubility of gas is calculated using (Parkhurst and Appelo, 2013),

$$m_i = K\varphi_i P_i/\gamma_i \quad (2)$$

where, m_i is the solubility of gas species, K is the equilibrium constant, φ_i is the fugacity factor, P_i is the partial pressure, and γ_i is the activity coefficient in the aqueous phase.

The dissolution kinetic of calcite ($CaCO_3$) was modelled using PHREEQC using the following kinetic reaction and temperature dependent constants,

$$R_k = 167\left(\frac{m}{m_0}\right)^n (\alpha_H + K_1 + \alpha_{CO2}K_2 + \alpha_{H2O}K_3)(1 - 10^{nSI_{CaCO3}}) \quad (3)$$

$$K_1 = 10^{(0.198-\frac{444}{T})}, \qquad K_2 = 10^{(2.84-\frac{2177}{T})}, \qquad K_3 = \begin{cases} 10^{(-5.86-\frac{317}{T})}, & T \le 298 \\ 10^{(-1.1-\frac{1737}{T})}, & T > 298 \end{cases}$$

where $(m/m_0)^n$ is the factor to account for any changes in the initial surface area of the solid (calcite) during dissolution, default numbers were taken from Plummer et al. (1978), α is the activity of each calcite species, n was taken as 0.67, representing uniformly dissolving spheres (Parkhurst & Appelo, 2013), and K_1, K_2, K_3 are temperature dependent.

Assuming carbonate equilibria $CO_2(g) = CO_2(aq)$ and considering only the temperature, the partial pressure (pCO_2) was calculated for the seventeen well fluids previously analysed (Table 4). Dissolved carbonate is assumed to be distributed among the carbonate and bicarbonate ions ($CO_3^{2-}$and HCO_3^-) and aqueous carbon dioxide ($CO_2(aq)$). In general, [Tot-CO_3^{2-}] is the sum of the individual ion concentrations ([HCO_3^-] + [CO_2] + [CO_3^{2-}]). The partial pressure of carbon dioxide (pCO_2) was calculated directly from the reaction $CO_2(g) \leftrightharpoons CO_2(aq)$. The predicted partial pressure of carbon dioxide (Table 4) agrees well with the observations of Satman et al. (2020), who reported low carbon dioxide content in shallow and old wells (KD-23B until R-5A). This also illustrates the effect of drop-in CO_2 solubility when pressure is reduced.

4.3. Estimation of synthetic geothermal fluid composition

The data for R-3A and R-5A production wells, which are very close to the selected field observation wells in the project, were selected to calculate the maximum CO_2 concentration that can be dissolved under high T and P through geochemical equilibrium modelling. A gas-water exchange reaction was coded in PHREEQC. Input data for the initial solution included temperature, redox conditions, and concentrations of analysed chemical components, except for pH, and the predicted initial pCO_2 results (Table 4). As redox potential specifies the redox conditions and distributes the redox elements among its valence states, pe (the relative tendency of the solution to accept or give electrons) was taken from relevant published literature (Müller and Regenspurg, 2017). Müller and Regenspurg (2017) measured pe on thermal water samples as 3.3 for oxic brine and 1.8 for anoxic brine. Since bicarbonate-rich waters, in general, originate either from dissolution CO_2 gas or condensation of geothermal steam in relatively deep, oxygen free ground waters, a pe of 1.8 is considered to reflect well the conditions of the studied wells.

Major cations (K^+, Na^+, Ca^{2+}) and major anions (Cl^-, SO_4^{2-} and CO_3^{2-}) concentrations in R-3A and R-5A wells (Table 4) were used to back-calculate the composition of synthetic brine that was used in the high-pressure high-temperature laboratory experiments. A relatively simple brine comprising of Na_2SO_4, KCl and $CaCO_3$ salts (Table 5) was shown to provide a reasonable approximation of ion concentrations in the previously analysed fluids. For Na_2SO_4, based on Na^+ and SO_4^{2-} ion concentrations for both the wells, the calculated Na_2SO_4 concentration ranged between 850 – 3,830 mg l^{-1}. For KCl, two different sets of calculations were made to determine the K^+ and Cl^- ion concentrations separately. The calculation suggested a KCl concentration between 222 – 750 mg l^{-1} for R-3A well and 150 – 370 mg l^{-1} for the R-5A well. This agrees well with the increased solubility of KCl at high temperatures, particularly >568 mg l^{-1} above 100 ˚C. The higher concentration of KCl was used in the synthetic brine. For $CaCO_3$, based on $Ca^{2+}$and CO_3^{2-} ion concentration for both wells, the calculated $CaCO_3$ concentration was around ~5.7 mg l^{-1}. This is very close to the solubility product constant K_{sp}= 4.5×10^{-9} ($CaCO_3 = [Ca^{2+}][CO_3^{2-}]$), the equilibrium constant for the solid substance dissolved in an aqueous solution (Segnit et al., 1962). Particularly, the lower range of concentrations is indicative of waters not being fully saturated in terms of Na_2SO_4 and KCl, whereas for $CaCO_3$ it represents a fully saturated solution. A rounded average range value for each salt (column w in Table 5) was selected to prepare the synthetic brine by dissolving high purity solid Sodium sulphate, Potassium chloride and Calcium carbonate salts in deionised water. The PHREEQC model was set up by assigning the synthetic brine composition as the initial solution.

Table 5: Synthetic brine composition (mg l^{-1}) estimated using PHREEQC.

Salt	Range for R-3A and R-5A	w
Sodium sulphate (Na_2SO_4)	850 – 3,830	2,000
Potassium chloride (KCl)	222 – 750	500
Calcium carbonate ($CaCO_3$)	5.7	5.7

5. ANALYSIS AND MODELLING OF GEOCHEMICAL AND PHYSICAL CHANGES FOLLOWING THE FIRST STAGE REACTOR EXPERIMENTS

One of the five reactors, which contained marble cores A-VIII, B-VI and C-VII, was removed from the experimental set up after completion of the first stage HPHT experiments. Post-reactor experiment μ-CT scanning of the core samples was followed by the chemical analysis of the reactor brine in order to establish the effects of exposure to synthetic reservoir brine charged with 4% CO_2 under initial reservoir conditions. Figure 1

Geochemical equilibrium modelling using PHREEQC was carried out to establish equilibrium between the brine collected from the opened reactor and the most abundant mineral phase following the first stage experiments. This was performed to identify any dissolution/precipitation reactions that would have taken place, as well any changes in the composition of the synthetic brine used in the reactor experiments. Saturations indexes of the potential minerals controlling fluid-rock interactions were estimated in PHREEQC.

Brine analysis from the reactor containing marble cores was then used to compare actual changes of brine composition with the modelling predictions and support the investigation of reservoir rock and fluids interaction under reservoir conditions simulated in the laboratory using the rector experiments, geochemical analysis and modelling. pH and electrical conductivity were measured immediately after exposure to air. For the brine analyses (geochemical characterisation) samples were stored in plastic (HDPE) containers and analyses were performed. The analytical method used for alkalinity (as $HHCO_3^-$) involved the use of a 100-200 ml sample volume to measure alkalinity by titration. All remaining brine samples were transported in 50 ml containers. At the time of sampling, nitric acid was added to the samples of metals and major cations to acidify the samples at pH between 1-2 and therefore stabilise these ions in the solution. Concentrations of metals, major cations (K^+, Na^+, Ca^{2+}, and Mg^{2+}) and anions (SO_4^{2-} and Cl^-) in the aqueous samples were determined using inductively coupled plasma optical emission spectrometry (Perkin Elmer/Optima 2100 DV) and liquid chromatography by ions (Dionex/RCS 1000), respectively.

The following paragraphs outline the observed changes in geochemistry of the reactor fluids, given the exposure of the marble cores to the synthetic brine at both under the reservoir pressure and temperature and atmospheric conditions. Geochemical equilibrium modelling with PHREEQC between the brine, CO_2 and the mineral phase was used to estimate the geochemical changes taking place post-reservoir fluids exposure at reservoir pressure and temperature conditions (while the reactors are sealed) and any change once the canisters are opened and samples are removed (atmospheric temperature and pressure). This is helpful to see whether the dissolved CO_2 in brine after injection causes minerals to dissolve and precipitate and any changes in the mineral composition at different stages. A three-step approach was also conducted in the modelling; at first the brine itself in the absence of CO_2 was modeled, then the dissolved CO_2 in brine was modelled and finally by assuming chemical equilibrium with calcite.

The calcite saturation index (SI_{CaCO_3}) was -1.1 for the initial solution, while the final value predicted using PHREEQC is 0.33 indicating the dissolution of solid calcite which leads to release of Ca^{2+} and CO_3^{2-} ions ($CaCO_{3(solid)} \leftrightharpoons Ca^{2+} + CO_3^{2-}$). The produced carbonate ions improve the buffering capacity of the system by increasing HCO_3^- and decreasing the H^+ ion concentration, which resist the system against pH-variation. Calcite dissolution occurs normally when the solution is under-saturated for either Ca^{2+} or CO_3^{2-} ions and the presence of these ions together with CO_2 in the brine formation could affect the calcite dissolution significantly. As CO_2 was injected in the brine solution, batch reaction calculations, based on experimental T and P, showed an increase in calcite saturation index. It can be seen from Table 6 that except for Calcite, Chalcedony and Quartz, all other minerals are under saturated (negative SI values). The predicted supersaturation for Chalcedony and Quartz is low (0.07 and 0.13 respectively), while the relative saturation of Calcite (0.33) is approximately three times larger. The same was observed by previous researchers (Hangx et al., 2013; Lamy-Chappuis et al., 2016), who attributed strong grain to grain contact in Quartz to be the main reason for exhibiting minor changes as compared to Calcite that undergoes significant dissolution and microstructural changes. This explains why calcite scaling is a common problem in geothermal reservoirs as regularly observed in the field. The physical effect of positive SI values would be observed as precipitation of the three minerals on the surface and pore spaces within the marble cores, while it is expected that minerals for which predicted SI values are negative would dissolve with a stronger dissolution rate for the more highly negative SI values.

The aqueous solution is shown to reach local equilibrium while rock minerals, calcite and water composition keep changing after equilibration. The dissolution kinetics of minerals are mainly dependent on *in situ* water formation and temperature although rock composition could also affect the reactive transport processes. The equilibration time is inversely proportional to temperature. It was observed that the rate of calcite dissolution was very fast (in the order of a few hours) and the reaction rate further increased at higher pressure, where more Ca^{2+} and CO_3^{2-} are released and the buffering of the system improves. Khalediali dusti & Kleppe (2017) studied the effect of pressure on CO_2 dissolution in water and found that CO_2 will dissolve in aqueous phase at higher reservoir pressure, which in turn increases the calcite dissolution rate. Thus, it can be inferred that in case of high CO_2 concentration/pressure in the geothermal wells, more calcite scaling will be observed and calcite dissolution can be used to control the pH of the geothermal reservoirs.

Table 6: Post-reservoir fluids exposure Saturation Indices (SI) for the mineral phases estimated using PHREEQC.

Mineral Name	SI
Anhydrite ($CaSO_4$)	-0.65
Aragonite ($CaCO_3$)	-0.04
Arcanite (K_2SO_4)	-5.75
Bloedite ($Na_2Mg(SO_4)_2 + 4H_2O$)	-11.91
Calcite ($CaCO_3$)	0.33
Chalcedony (SiO_2)	0.07
Dolomite ($CaMg(CO_3)_2$)	-3.91
Epsomite ($MgSO_4 + 7H_2O$)	-7.00
Halite (NaCl)	-5.21
Magnesite ($MgCO_3$)	-3.79
Mirabilite ($Na_2SO_4 + 10H_2O$)	-3.66
Quartz (SiO_2)	0.13
Sylvite (KCl)	-6.37
Thenardite (Na_2SO_4)	-3.60

Two different test conditions were chosen for the geochemical modelling. First the PHREEQC model was run for the experimental conditions (T= 200 ˚C and high pressure, P = 136 atm) and a second model run was implemented for atmospheric T and P, simulating the conditions when the reactors are initially shut and later opened, at which time the cores are removed and the canister reactor fluids are exposed to ambient atmospheric conditions. The pitzer.dat thermodynamic database was used for the modelling under the experimental conditions (at high T and P), while the phreeqc.dat database was used for atmospheric conditions (Appelo et al., 2014). Modelling the brine composition with the most abundant mineral phase (Calcite), the elements in solution (Table 7) and the predicted mineral phases (

PHREEQC predicted concentration under atmospheric conditions (after CO_2 injection) were compared with the analytical measurements, and it was found that the results were comparable for anions (Table 7). However, the analytical measurement values for cations are ~30% higher than that predicted by PHREEQC. This bias is currently being investigated in the model to understand the reaction kinetics suppressing the cations measurement. The saturation indices (**Fehler! Ungültiger Eigenverweis auf Textmarke.**) showed minor variations for most of the mineral phases, which can be attributed to the fact that the reaction kinetics of some mineral phases will be faster under the experimental conditions of high pressure and high temperature as compared to the atmospheric conditions. The main difference under the solution elements can be seen in sulphates and carbonates, where sulphates and carbonates are expected to be higher in solution under atmospheric conditions compared to the conditions under high T and P. Most of the mineral phases of sulphates and carbonates were under-saturated under the atmospheric conditions. For example, misenite ($K_8H_6(SO_4)_7$), portlandite ($Na_2Ca(CO_3)_2 + 2H_2O$), and thenardite (Na_2SO_4) showed a higher dissolution rate under the atmospheric conditions, which suggests that water will try to dissolve these elements to reach equilibrium. However, in the case of, anhydrite ($CaSO_4$), it was under-saturated in atmospheric conditions, while it would precipitate in the experimental conditions. This observation explains the substantially higher sulphate content predicted in solution for the brine in atmospheric conditions, which is indeed in good agreement with the analytical measurement (Table 7). All other minerals had similar behaviour under experiment and atmospheric conditions.

The pH and conductivity of the brine solution was also modelled in PHREEQC (Table 9). The values were modelled at different steps, i.e., when there is only brine solution, when the solution has equilibrated with calcite and finally after CO_2 injection under atmospheric conditions. The brine solution is estimated to turn alkaline at equilibrium with calcite, and the pH is expected to increase from 9.7 to 10. This is considered reasonable as calcite dissolution is very effective in controlling the pH of the system. However, the conductivity of the brine solution is not predicted to change appreciably. The brine solution is expected to turn towards neutral ($pH = 7$) after CO_2 injection. This can be attributed to the fact that CO_2 will dissolve in the solution at high pressure and high temperature to create acidic ions, thereby neutralising the alkalinity of the solution. The conductivity of the solution is also estimated to increase by ~0.1 mS/cm, which can be attributed to the presence of free ions in the solution. The modelled pH and conductivity was compared with the analytical measurements after CO_2 injection. The values estimated through the PHREEQC model and those from analytical measurements are in good agreement, suggesting the PHREEQC modelling provides a very good representation of the experimental setting.

Table 8) were obtained under experimental and atmospheric conditions based on the bulk composition of XRD analysis, together with CO_2 to equilibrate with the brine solution. These are compared with the chemical analysis results for the fluid sampled from the first reactor which housed marble cores A-VIII, B-VI and C-VII.

Table 7: Predicted PHREEQC brine solution composition under experimental HT-HP and atmospheric conditions compared with the analytical measurements (NA: Not applicable as it was not measured; ND: Not Detected)

Element Name	Experimental conditions (mg l^{-1})	Atmospheric conditions (mg l^{-1})	Analytical measurements (mg l^{-1})
Calcium (Ca^{2+})	75	75	105
Sodium (Na^{+})	344	344	476
Potassium (K^{+})	81	81	140
Chloride (Cl^{-})	73.7	73.7	77.7
Sulphur (S)	140	140	NA
Sulphates (SO_4^{2-})	256	450	459

Carbonates (CO_3^{2-})	0.03	3.3	ND

PHREEQC predicted concentration under atmospheric conditions (after CO_2 injection) were compared with the analytical measurements, and it was found that the results were comparable for anions (Table 7). However, the analytical measurement values for cations are ~30% higher than that predicted by PHREEQC. This bias is currently being investigated in the model to understand the reaction kinetics suppressing the cations measurement. The saturation indices (**Fehler! Ungültiger Eigenverweis auf Textmarke.**) showed minor variations for most of the mineral phases, which can be attributed to the fact that the reaction kinetics of some mineral phases will be faster under the experimental conditions of high pressure and high temperature as compared to the atmospheric conditions. The main difference under the solution elements can be seen in sulphates and carbonates, where sulphates and carbonates are expected to be higher in solution under atmospheric conditions compared to the conditions under high T and P. Most of the mineral phases of sulphates and carbonates were under-saturated under the atmospheric conditions. For example, misenite ($K_8H_6(SO_4)_7$), portlandite ($Na_2Ca(CO_3)_2 + 2H_2O$), and thenardite (Na_2SO_4) showed a higher dissolution rate under the atmospheric conditions, which suggests that water will try to dissolve these elements to reach equilibrium. However, in the case of, anhydrite ($CaSO_4$), it was under-saturated in atmospheric conditions, while it would precipitate in the experimental conditions. This observation explains the substantially higher sulphate content predicted in solution for the brine in atmospheric conditions, which is indeed in good agreement with the analytical measurement (Table 7). All other minerals had similar behaviour under experiment and atmospheric conditions.

The pH and conductivity of the brine solution was also modelled in PHREEQC (Table 9). The values were modelled at different steps, i.e., when there is only brine solution, when the solution has equilibrated with calcite and finally after CO_2 injection under atmospheric conditions. The brine solution is estimated to turn alkaline at equilibrium with calcite, and the pH is expected to increase from 9.7 to 10. This is considered reasonable as calcite dissolution is very effective in controlling the pH of the system. However, the conductivity of the brine solution is not predicted to change appreciably. The brine solution is expected to turn towards neutral ($pH = 7$) after CO_2 injection. This can be attributed to the fact that CO_2 will dissolve in the solution at high pressure and high temperature to create acidic ions, thereby neutralising the alkalinity of the solution. The conductivity of the solution is also estimated to increase by ~0.1 mS/cm, which can be attributed to the presence of free ions in the solution. The modelled pH and conductivity was compared with the analytical measurements after CO_2 injection. The values estimated through the PHREEQC model and those from analytical measurements are in good agreement, suggesting the PHREEQC modelling provides a very good representation of the experimental setting.

Table 8: Predicted mineral phases under experimental and atmospheric conditions

Mineral Name and phase	Experimental conditions (*SI*)	Atmospheric conditions (*SI*)
Anhydrite ($CaSO_4$)	0.40	-0.96
Aragonite ($CaCO_3$)	-0.37	-0.26
Arcanite (K_2SO_4)	-4.96	-4.69
Burkeite ($Na_6CO_3(SO_4)_2$)	-21.59	-18.63
Calcite ($CaCO_3$)	0.00	0.00
Chalcedony (SiO_2)	-0.06	-0.45
Carbon dioxide ($CO_2(g)$)	-1.40	--
Glaserite ($CaNa_2(CO_3)_2 + 5H_2O$)	-13.05	-7.70
Glaserite ($NaK_3(SO_4)_2$)	-11.43	-8.76
Glauberite ($Na_2Ca_5(SO_4)_2$)	-2.90	-5.20
Goergeyite ($K_2Ca_5(SO_4)_6H_2O$)	-2.11	-2.71
Gypsum ($CaSO_4 + 2H_2O$)	-0.98	-0.55
Halite (NaCl)	-5.01	-5.34
Kalicinite ($KHCO_3$)	-6.91	-4.81
Mirabilite ($Na_2SO_4 + 10H_2O$)	-3.70	-3.91
Misenite ($K_8H_6(SO_4)_7$)	-3.70	-64.52
Nahcolite ($NaHCO_3$)	-5.55	-3.38
Natron ($Na_2CO_3 + 10H_2O$)	-9.55	-7.85
Portlandite ($Na_2Ca(CO_3)_2 + 2H_2O$)	-7.43	-12.03
Sylvite (KCl)	-5.74	-5.25
Thenardite (Na_2SO_4)	-3.69	-5.09

Table 9: Predicted PHREEQC and analytical measurements of pH and conductivity (mS/cm)

Steps	Modelled		Analytical	
	pH	Conductivity	pH	Conductivity
Only brine	9.7	3.923	--	--
In equilibrium with calcite	10	3.943	--	--
After CO_2 injection	7.4	4.050	6.96	4.0

Porosity measurements carried out on marble samples have shown significant increase after HPHT treatment and exposure to reservoir brine charged with 4% CO_2 (Table 10). Based on the Saturation Indexes estimated at experimental conditions (Table 8), the most carbonate minerals show a higher tendency to dissolve, with the calcite reaction rate being the highest. These dissolution kinetics

under the experimental conditions, are expected to manifest as transformation on mineral grain surfaces which also affect the pore space. Figure 7 presents the μ-CT images of the Kızıldere marble core sample C-VII before and after the first stage HPHT reactor treatment. The surface of the core clearly indicates dissolution which is more prominent and visible on the rough more porous regions of the core specimen (darker coloured regions), which appear etched. Although mineralogical analysis has not been carried out yet, it is expected that the displaced material is likely carbonate minerals, as the geochemical equilibrium modelling indicates (positive SI) in Table 8. It is therefore considered reasonable to observe an increase in porosity of the marble cores, attributed to the long-term exposure of the marble rocks to acidic environment, which can induce acid etching (surface corrosion) as well as due to the dissolution of calcite in the synthetic brine. Xu et al. (2007) and Tan et al. (2022) also showed that the dissolved high-pressure CO_2, that is being injected, enhance mineral alteration, particularly carbonate dissolution and showed significant increases in porosity took place in the acidified zone where mineral dissolution occurs.

Table 10. Porosities of marble samples before and after high pressure high temperature treatment.

Sample	Before	After	% Increase
Marble A. V.3	6.00%	20.60%	243
Marble B VI	11.30%	20.80%	84
Marble C VII	7.00%	11.90%	70

These preliminary results obtained from geochemical analysis as well as laboratory analysis matches well with the previous researchers and observations made in the field, which suggest the geochemical modelling are a true representation of the geothermal wells. A detailed analysis of the change in geochemical, geomechanical and geophysical properties of all the samples will be reported once the long-term high pressure high temperature experiment is completed.

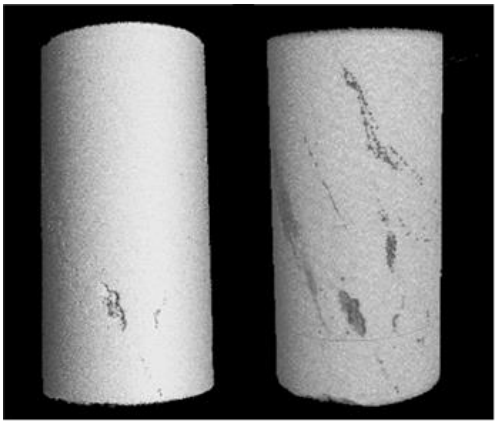

(a) (b)

Figure 7: μ-CT images of the Kızıldere marble core sample C-VII (a) before and (b) after the first stage HPHT reactor treatment under pre-production reservoir brine and CO_2 concentration conditions.

6. CONCLUSIONS

Long term high pressure high temperature experiments were undertaken to analyse the effect of CO_2-brine-rock interactions on the geochemical, geomechanical and geophysical properties of Kizildere marbles. The geochemical modelling between the brine, CO_2 and the mineral phase to estimate the geochemical changes taking place at the post-reservoir fluids exposure under reservoir pressure and temperature conditions showed reaction kinetics of some mineral phases being faster under reservoir pressure and temperature conditions compared to the atmospheric conditions. When the brine analysis was compared with the modelling predictions, the predicted concentrations, especially for the anions, were quite similar to the analytical measurements under atmospheric conditions (after injection). The higher sulphates concentration under both the predicted and the analytical measurements are explained by the higher dissolution rate of the anhydrite under these conditions. The brine composition predicted by PHREEQC estimated a pH increase when the solution was modelled under equilibrium with calcite. This is considered reasonable as calcite dissolution is very effective in controlling the system. When CO_2 was injected, pH decreased due to the fact that CO_2 is dissolved in the solution at high pressure and temperature, creating acidic ions. The values estimated through the PHREEQC model and those from analytical measurements were in good agreement, suggesting that PHREEQC modelling provides a good representation of the experimental set up. Increased porosity measurements on the rock mineral after reservoir-fluid exposure also validate the higher dissolution rate for carbonate minerals under the experimental conditions; where high-pressure dissolved CO_2 can induce mineral dissolution and therefore alter pore space. A comparison of the baseline properties of marble samples with the change in geochemical, geomechanical and geophysical properties of the treated marble samples will be carried out in the future.

ACKNOWLEDGEMENTS

SUCCEED is funded through the ACT programme (Accelerating CCS Technologies, Horizon 2020 Project No 294766). Financial contributions made by the Department for Business, Energy & Industrial Strategy UK (BEIS), the Rijksdienst voor Ondernemend Nederland (RVO), the Scientific and Technological Research Council of Turkey (TUBITAK), and our research partners Orkuveita

Reykjavíkur/Reykjavik Energy Iceland (OR) and Istituto Nazionale di Oceanografia e di Geofisica Sperimentale Italy (OGS) are gratefully acknowledged. The authors are also thankful to Graham Nash and Gary Jones of Imperial College London for their contributions towards the construction of the HPHT reactor set up and the experiments. Ellen Meijvogel-de Koning of the Department of Applied Geophysics and Petrophysics, Delft University of Technology carried out μ-CT scanning of all the core samples pre- and post-reactor experiments. Derya Gökçe, Emrah Soysal and Egemen Güler of the Petroleum Research Center, Middle East Technical University conducted the chemical analysis of the post-reactor experiment brine presented in this paper.

REFERENCES

Addassi, M., Omar, A., GHorayeb, K. & Hoteit, H. Comparison of various reactive transport simulators for geological carbon sequestration. *International Journal of Greenhouse Gas Control*, 110, 103419.

Akin, S., Yeltekin, K. & Parlaktuna, M. Numerical modeling of Kızıldere geothermal field, Turkey. European Geothermal Conference, 2003 Szeged, Hungary. 7p.

Aksoy, N., Gok, O. S., Mutlu, H. & Kılınc, G. CO_2 emission from geothermal power plants in Turkey. World Geothermal Congress, 2015 Melbourne, Australia. 7p.

Appelo, C. A. J., Parkhurst, D. L. & Post, V. E. A. 2014. Equations for calculating hydrogeochemical reactions of minerals and gases such as CO_2 at high pressures and temperatures. *Geochimica et Cosmochimica Acta,* 125**,** 49-67.

Appelo, C. A. J. & Postma, D. 2005. *Geochemistry, Groundwater and Pollution*, Taylor & Francis Group.

ESMAP 2016. Greenhouse gases from geothermal power production. *Technical Report 009/16*. Washington DC, USA: The World Bank Group.

Garg, S. K., Haizlip, J., Bloomfield, K. K., Kindap, A., Haklıdır , F. S. T. & Guney, A. A numerical model of the Kızıldere geothermal field, Turkey. World Geothermal Congress, 2015 Melbourne, Australia. 15p.

Haizlip, J. R., Stover, M. M., Garg, S. K., Haklıdır, F. S. T. & Prina, N. Origin and impacts of high concentrations of carbon dioxide in geothermal fluids of western Turkey. 41st Workshop on Geothermal Reservoir Engineering, 2016 Stanford, California. Stanford University, 11p.

Haklıdır, F. S. T., Akın, T., Güney, A. & Bükülmez, A. A. Geochemistry of fluids in new wells of Kızıldere geothermal field in Turkey. Thirty-Sixth workshop on Geothermal Reservoir Engineering, 2011 Stanford, Calfornia, USA. Stanford University, 8p.

Haklidir, F.T, Sengun, R. Haizlip, J. R. 2015. The Geochemistry of the Deep Reservoir Wells in Kizildere (Denizli City) Geothermal Field(Turkey). Proceedings World Geothermal Congress 2015, Melbourne, Australia, 19-25 April 2015

Hangx, S., Van Der Linden, A., Marcelis, F. & Bauer, A. 2013. The effect of CO_2 on the mechanical properties of the captain sandstone: geological storage of CO_2 at the Goldeneye field (UK). *International Journal of Greenhouse Gas Control,* 19**,** 609-619.

Hao, Y., Smith, M., Sholokhova, Y. & Carroll, S. 2013. CO_2-induced dissolution of low permeability carbonates. Part II: Numerical modelling of experiments. *Advances in Water Resources,* 62**,** 388-408.

Hassler, G. L. 1944. *Method and apparatus for permeability measurements*. US 2345935 A. 4 April 1944.

Holm, A., Jennejohn, D. & Blodgett, L. 2012. *Geothermal energy and greenhouse gas emissions*, Geothermal Energy Association.

Jahanbakhsh, A., Liu, Q., Hadi Mosleh, M., Agrawal, H., Farooqui, N. M., Buckman, J., Recasens, M., Maroto-Valer, M., Korre, A. & Durucan, S. 2021. An investigation into CO_2–brine–cement–reservoir rock interactions for wellbore integrity in CO_2 geological storage. *Energies,* 14**,** 5033.

Jahanbakhsh, A., Recasens, M., Farooqui, N. M., Maroto-Valer, M. M., Mosleh, M. H., Agrawal, H., Korre, A. & Durucan, S. An investigation into CO_2-brine-cement-caprock interactions for wellbore integrity in CO_2 geological storage. 14th International Conference on Greenhouse Gas Control Technologies, 2018 Melbourne, Australia. GHGT-14, 5p.

Khaledialidusti, R. & Kleppe, J. Significance of the kinetics of minerals in reactive-transport problems. 79th EAGE Conference and Exhibition, 2017 Paris, France. Society of Petroleum Engineers.

Koederitz, L., Harvey, A. H. & Honarpour, M. 1989. *Introduction to petroleum reservoir analysis contributions in petroleum geology & engineering*, Gulf Publishing Company.

Kovari, K. & Tisa, A. 1975. Multiple failure state and strain controlled triaxial tests. *Rock Mechanics,* 7**,** 17-33.

Lamy-Chappuis, B., Angus, D., Fisher, Q. J. & Yardley, B. W. D. 2016. The effect of CO_2-enriched brine injection on the mechanical properties of calcite-bearing sandstone. *International Journal of Greenhouse Gas Control,* 52**,** 84-95.

Layman, E. B. Geothermal projects in Turkey: Extreme greenhouse gas emission rates comparable to or exceeding those from coal-fired plants. 42nd Workshop on Geothermal Reservoir Engineering, 2017 Stanford, California. Stanford University, 16p.

Müller, D. R. & Regenspurg, S. 2017. The element-release mechanisms of two pyrite-bearing siliciclastic rocks from the north german basin at temperatures up to 90 °C under oxic and anoxic conditions. *Geothermal Energy,* 5p.

Nehler, M., Andolfsson, T., Renner, J., Steeb, H. & Bracke, R. Laboratory setups for core flooding and CT scanning experiments at in-situ HP/HT conditions. World Geothermal Congress, 2015 Melbourne, Australia. 7p.

Parkhurst, D. L. & Appelo, C. A. J. 2013. *Description of input and examples for PHREEQC version 3—a computer program for speciation, batch-reaction, one-dimensional transport, and inverse geochemical calculations, Chapter 43 of Section A, Groundwater book 6, Modeling Techniques*, U.S. Geological Survey.

Peter, A., Yang, D., Eshiet, K. I.-I. I. & Sheng, Y. 2022. A Review of the studies on CO_2–brine–rock interaction in geological storage process. *Geosciences,* 12**,** 168.

Pham, V. T. H., Lu, P., Aagaard, P., Zhu, C. & Hellevang, H. 2011. On the potential of CO_2–water-rock interactions for CO_2 storage using a modified kinetic model. *International Journal of Greenhouse Gas Control,* 5**,** 1002-1015.

Pimienta, L., Esteban, L., Sarout, J., Liu, K., Dautriat, J., Delle Piane, C. & Clennell, M. B. 2017. Supercritical CO_2 injection and residence time in fluid-saturated rocks: evidence for calcite dissolution and effects on rock integrity. *International Journal of Greenhouse Gas Control,* 67**,** 31-48.

Piper, A. M. 1944. A Graphic procedure in the geochemical interpretation of water analyses. *Transactions, American Geophysical Union***,** 914-928.

Plummer, L. N., Wigley, T. M. L. & Parkhurst, D. L. 1978. The kinetics of calcite dissolution in CO_2 - water systems at 5 degrees to 60 degrees C and 0.0 to 1.0 atm CO_2. *American Journal of Science,* 278 (2), 179-216.

Pruess, K. 2006. Enhanced Geothermal Systems (EGS) using CO_2 as working fluid—a novel approach for generating renewable energy with simultaneous sequestration of carbon. *Geothermics,* 35**,** 351-367.

Rose, P., Xu, T., Kovac, K., Mella, M. & Pruess, K. Chemical stimulation in near-wellbore geothermal formations: silica dissolution in the presence of calcite at high temperature and high pH. Thirty-Second Workshop on Geothermal Reservoir Engineering, 2007 Stanford, California. Stanford University.

Salimi, H. & Wolf, K.-H. 2012. Integration of heat-energy recovery and carbon sequestration. *International Journal of Greenhouse Gas Control,* 6**,** 56-68.

Satman, A., Tureyen, O. I. & Basel, E. D. K. The carbon dioxide behavior of the Kızıldere geothermal field. Fourty-Second Workshop on Geothermal Reservoir Engineering, 2017 Stanford, California. Stanford University.

Satman, A., Tureyen, O. I., Basel, E. D. K., Guney, A., Senturk, E. & Kindap, A. Effect of carbon dioxide content on the well and reservoir performances in the Kizildere geothermal field. World Geothermal Congress, 2020 Reykjavik, Iceland. 6p.

Segnit, E.R., Holland, H.D., & Biscardi C.J. 1962. The solubility of calcite in aqueous solutions-I: The solubility of calcite in water between 75^{o}C and 200^{o}C at CO_2 pressures up to 60 atm. *Geochimica et Cosmochimica Acta*, 26 (12), 1301-1331.

Setiawan, M. R., Iqbal, M. & Siregar, R. N. 2018. Mineral analysis in rocks using XRD and Petrography. *Journal of Science and Applicative Technology***,** 206-214.

Shabani, A., Kalantariasl, A., Abbasi, S., Shahrabadi, A. & Aghaei, H. 2019. A coupled geochemical and fluid flow model to simulate permeability decline resulting from scale formation in porous media. *Applied Geochemistry,* 107**,** 131-141.

Shah, M., Sircar, A., Shaikh, N., Patel, K., Sharma, D. & Vaidya, D. 2018. Comprehensive geochemical/hydrochemical and geo-thermometry analysis of Unai geothermal field, Gujarat, India. *Acta Geochimica,* 38**,** 145-158.

Şimşek, Ş., Yıldırım, N. & Gülgör, A. 2005. Developmental and environmental effects of the Kızıldere geothermal power project, Turkey. *Geothermics,* 34**,** 234-251.

Sun, Y., Li, Q., Yang, D. & Liu, X. 2016. Laboratory core flooding experimental systems for CO_2 geosequestration: an updated review over the past decade. *Journal of Rock Mechanics and Geotechnical Engineering,* 8**,** 113-126.

Tale, F., Kalantariasl, A., Shabani, A., Abbasi, S., Zohoorian, A. H. & Khamehchi, E. 2020. Experimental and simulation study of low salinity brine interactions with carbonate rocks. *Journal of Petroleum Science and Engineering,* 184**,** 106497.

Tan, Y., Li, Q., Xu, L., Xu, L., Yu, T. & Cao, X. 2022. CO_2–brine–rock interaction and sequestration capacity in carbonate reservoirs of the Tahe oilfield. *Greenhouse Gases: Science and Technology*.

Valle, L. M., Grima, C., Rodríguez, R. & Llopis, C. 2020. Effect of $SCCO_2$-brine mixture on injectivity and storage capacity in rock samples of naturally fractured carbonate formations. *Journal of Natural Gas Science and Engineering,* 81**,** 103452.

Wallace, K., Dunford, T., Ralph, M. & Harvey, W. 2009. Germencik: A thoroughly modern flash plant in Turkey. *GRC Transactions,* 33p.

Wang, J., Zhao, Y., An, Z. & Shabani, A. 2022. CO_2 storage in carbonate rocks: an experimental and geochemical modelling study. *Journal of Geochemical Exploration,* 234**,** 106942.

Xu, T., Apps, J.A., Karsten Pruess, K. & Yamamoto, H. 2007. Numerical Modelling of Injection and Mineral Trapping of CO_2 with H_2S and SO_2 in a Sandstone Formation. *Chemical Geology,* 242 (3-4), 319-346.

Zhang, B. A., Li, X. M. & Zhang, D. M. 2021. Study on mechanical and permeability characteristics of containing gas coal-rock under conventional triaxial compression. *Geotechnical and Geological Engineering*.

Zhang, G., Lu, P., Zhang, Y., Tu, K. & Zhu, C. 2020. SUPPHREEQC: A program for generating customized PHREEQC thermodynamic datasets from supcrtbl and extending calculations to elevated pressures and temperatures. *Computers & Geosciences,* 143**,** 104560.

Zhang, L., Zhang, C., Tu, S., Tu, H. & Wang, C. 2015. A study of directional permeability and gas injection to flush coal seam gas testing apparatus and method. *Transport in Porous Media,* 111**,** 573-589.

Zhu, C. & Anderson G. 2002. Environmental applications of geochemical modeling. Cambridge University Press, Cambridge.

Zhu, J., Parris, T. M., Richard Bowersox, J. & Harris, D. C. 2013. Modelling CO_2–brine–rock interactions in the Knox group: implications of a deep carbon storage field test in western Kentucky. *Applied Geochemistry,* 37**,** 29-42.

Zou, Y., Zheng, C. & Sheikhi, S. 2021. Role of ion exchange in the brine-rock interaction systems: a detailed geochemical modelling study. *Chemical Geology,* 559**,** 119992.